# Modelling electron-phonon interactions in graphene with curved space hydrodynamics

**I.Giordanelli[1,*], M. Mendoza[1], and H. J. Herrmann[1,2]**

[1]ETH Zürich, Computational Physics for Engineering Materials, Institute for Building Materials, Wolfgang-Pauli-Strasse 27, HIT, CH-8093 Zürich, Switzerland
[2]Universidade Federal do Ceará, Departamento de Física, Campus do Pici, 60455-760 Fortaleza, Ceará, Brazil
[*]gilario@ethz.ch

## ABSTRACT

We introduce a different perspective describing electron-phonon interactions in graphene based on curved space hydrodynamics. Interactions of phonons with charge carriers increase the electrical resistivity of the material. Our approach captures the lattice vibrations as curvature changes in the space through which electrons move following hydrodynamic equations. In this picture, inertial corrections to the electronic flow arise naturally effectively producing electron-phonon interactions. The strength of the interaction is controlled by a coupling constant, which is temperature independent. We apply this model to graphene and recover satisfactorily the linear scaling law for the resistivity that is expected at high temperatures. Our findings open up a new perspective of treating electron-phonon interactions in graphene, and also in other materials where electrons can be described by the Fermi liquid theory.

## 1 Introduction

At finite temperatures, phonons interact with charge carriers, and therefore, contribute to the electrical resistivity of the respective material.[1] For most solids, the temperature behaviour of the electrical resistivity changes at the Debye temperature, which corresponds to the theoretical highest phonon frequency in the material. In graphene, the Debye temperature is very high, $T \approx 2300$ K and $T \approx 1300$ K for planar and out-of-plane phonons, respectively.[2] However, for low electron densities, the Fermi energy can be substantially smaller than the Debye energy, and only phonons with energy smaller than two times the Fermi energy, corresponding to a full backscattering of electrons, can scatter with the electrons. This defines the Bloch-Gruňeisen temperature $T_{BG}$,[3] which for doped suspended graphene is around 100 K.[4,5] Therefore, in suspended graphene, the behaviour of the resistivity changes at Bloch-Gruňeisen temperature $T_{BG}$. It has been observed, that the temperature dependence of the resistivity follows a linear relation due to electron-phonon interactions above 100 K and even becomes quadratic in the absence of any external strain.[6,7]

Recently it has been shown that electronic flow in graphene can be modelled using relativistic hydrodynamic equations.[8–15] Usually, in this hydrodynamic formalism, electron-phonon interactions are included into the equation for the electrical current density $\vec{J}$ as a damping term, $-\vec{J}/\tau_p$, with a characteristic relaxation time $\tau_p$.[14,15] However, a proper inclusion of lattice-fluid interactions are missing. Here, we present a novel approach where we account for the electron-phonon interactions by including inertial corrections due to the deformations of the graphene sheet. We address the question whether these inertial corrections can recover the linear temperature relation of the electrical resistivity in the high temperature regime.

## 2 Method

We use molecular dynamics simulations to simulate different graphene membranes at different temperatures and imposed strains. From the position of the atoms, we build the coordinate system in which the electrons flow, and extract the inertial corrections to include them into the two-dimensional hydrodynamic equations. In Fig. 1, we can observe how the presence of thermal fluctuations produces curved streamlines of the electron velocity field.

To simulate the graphene sheets with molecular dynamics we use the adaptive intermolecular reactive bond-order (AIREBO) potential.[16] This many-body potential has been developed to simulate molecules made of carbon and hydrogen atoms, and has been very successful to reproduce the phonon dispersion curves of graphene.[17] In our simulations we consider suspended graphene sheets of $L_x = 99.2$ Å, (see Fig. 2), but also two stretched cases with 100.6 Å and 102.1 Å. As shown in Fig. 2 the zigzag edge is located along the $x$-direction (top and bottom) and accordingly the armchair edge along the $y$-direction (left and right). The atoms can freely move in all directions, except the ones at the left and right boundary, representing the electrical contacts (grey in Fig. 2). The distance between contacts will be denoted by $L_x$. Note that since the left and right
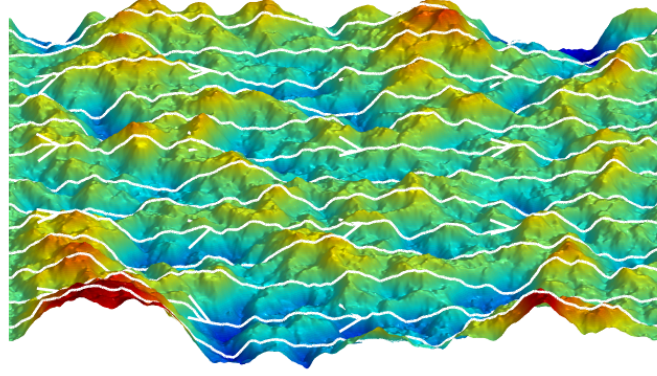
**Figure 1.** Graphene membrane at 300 K after the electronic flow has reached a steady state. Streamlines indicate the velocity field of the electronic flow that moves from left to right. The colours represent the height.

boundaries are fixed, we are effectively applying strain to the graphene samples, and therefore, expect a linear dependence of the resistivity with temperature. We simulate several samples at different temperatures within the range of 100-600 K controlling the temperature of the system with a Nosé-Hoover thermostat. All molecular dynamics simulations run (during the thermalisation procedure) with a time step $\Delta t = 1$ fs, which is small enough to capture the dynamics of the carbon-carbon interactions accurately. Randomised velocities are attributed to the atoms at the beginning of each simulation. After reaching thermal equilibrium we are ready to couple the graphene sheet to the fluid solver and introduce electrical currents.

The electronic flow in flat graphene can be modelled using relativistic hydrodynamic equations, which are responsible for the conservation of particles, $\partial_\mu N^\mu = 0$, and energy and momentum, $\partial_\mu T_0^{\mu\nu} = 0$, where $N^\mu$ and $T_0$ are the 3-particle flow and the energy-momentum tensor, respectively. The energy momentum tensor in Minkowski-space $T_0$ depends on the Minkowski metric $\eta_{\mu\nu}$ and the shear-stress tensor $\pi^{\mu\nu}$, which contains the shear viscosity $\kappa$. The equation of state completes this set of equations, which for the case of graphene is given by $\varepsilon = 2p$, where $\varepsilon$ is the energy density and $p$ the pressure. To take into account the curvature of suspended graphene sheets, we consider inertial corrections in these equations. For this purpose, we first use the covariant formulation of the hydrodynamic equations in curved space to determine the terms responsible for the inertial corrections, and afterwards, we introduce them as a forcing term into the respective equations for flat graphene. The conservation equations in curved manifolds are derived by replacing partial derivatives $\partial_\mu$ by covariant derivatives $\nabla_\mu$ and considering the energy-momentum tensor in curved space $T^{\mu\nu}$, which depends on the generalised metric $g_{\mu\nu}$ instead of the Minkowski (flat) metric $\eta_{\mu\nu}$. The covariant derivative $\nabla_\mu$ in the curvilinear coordinate system can be expressed through the respective partial derivative by $\nabla_\mu N^\mu = \partial_\mu N^\mu + \Gamma_{\mu\lambda}^\mu N^\lambda$, and $\nabla_\mu T^{\mu\nu} = \partial_\mu T^{\mu\nu} + \Gamma_{\mu\lambda}^\mu T^{\lambda\nu} + \Gamma_{\mu\lambda}^\nu T^{\mu\lambda}$, with $\Gamma_{\mu\lambda}^\mu$ being the Christoffel symbols, which are responsible for inertial corrections. With the help of the previous equations we can rewrite the inertial forces as

$$F_N = -\Gamma_{\mu\lambda}^\mu N^\lambda \tag{1a}$$

$$F_T^\nu = -\Gamma_{\mu\lambda}^\mu T_0^{\lambda\nu} - \Gamma_{\mu\lambda}^\nu T_0^{\mu\lambda} - (\eta^{\mu\nu} - g^{\mu\nu})\partial_\mu p, \tag{1b}$$

for the conservation of particles and energy-momentum, respectively. For more details on hydrodynamics in curved manifolds, see Ref.[18]

At this stage we include a temperature independent coupling constant $\alpha$ in front of the inertial corrections which accounts for the strength of the electron-phonon interaction. Thus, the set of equations can be written as

$$\partial_\mu N^\mu = \alpha F_N, \tag{2a}$$

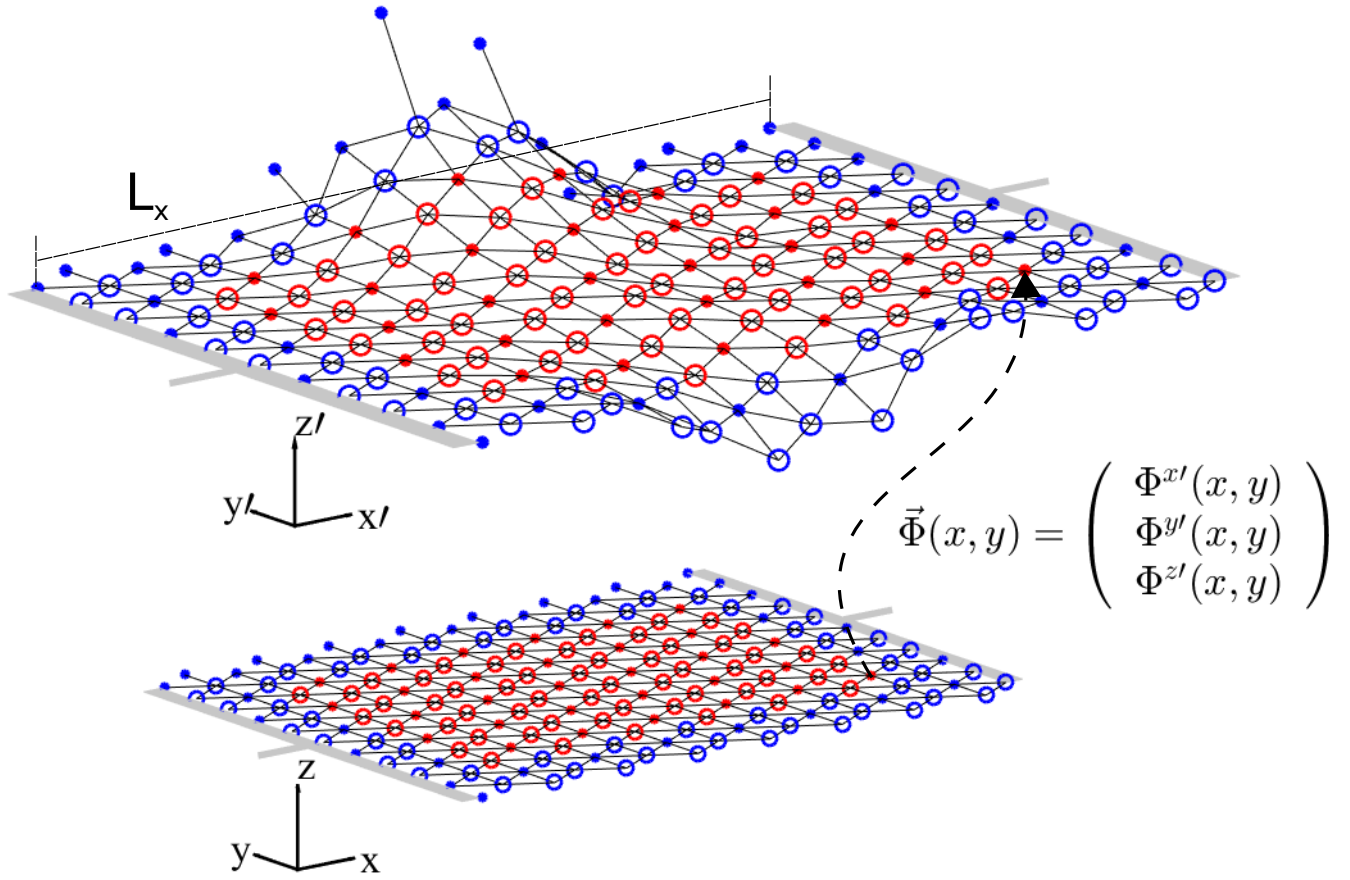$$\partial_\mu T_0^{\mu\nu} = \alpha F_T^\nu. \tag{2b}$$

**Figure 2.** Discrete mapping (dashed arrow) that describes the embedding of the two-dimensional triangular lattice (bottom figure) in the three-dimensional Cartesian space (top figure). The circles represent the atoms. The electrical contacts are shown in grey at both ends of the graphene sheet.

To solve these equations, we make use of the lattice Boltzmann solver described in Ref.,[13,19] and add the inertial contributions as external forces (see Additional Information for technical details on the numerical implementation). Our model discretises space as regular triangular lattice, which we couple to graphene's hexagonal lattice. As shown in Fig. 2, the atoms form a two-dimensional manifold which can be described by a discrete mapping $\Phi(ct,x,y)$ from the curved space to the three-dimensional flat space (reference frame of the laboratory, where the metric is given by the Minkowski-metric). The metric tensor can be computed by

$$g_{\mu\nu} = \frac{\partial \Phi^\alpha(ct,x,y)}{\partial x^\mu} \frac{\partial \Phi^\beta(ct,x,y)}{\partial x^\nu} \eta_{\alpha\beta}. \tag{3}$$

The graphene sheet possesses zigzag boundaries at the left and right end. For the fluid solver we impose periodic boundary conditions at these boundaries, which correspond to the in- and outlet. The free sides of the graphene sheet possesses armchair geometry and, therefore, we impose free slip boundary conditions.

We perform simulations in the Fermi liquid regime, in which the Fermi energy fixes the total number of charge carriers, and can determine whether electrons or holes dominate the charge carriers and electrical currents. Therefore, we set a constant particle density $n = 1.36 \times 10^{13}$ /cm$^2$ and compare our results with the experimental set-up proposed by Efetov et al.[4] We impose a constant particle density by coupling the fluid solver to a particle (charge) reservoir, thus fulfilling overall particle number conservation even for $\alpha \neq 1$. Therefore, at every time step during our simulations, we compensate the loss/gain of particles by injecting/subtracting charge carriers, such that the total number of particles is always conserved. This is on the line of the role of the gate voltage to fix the Fermi level and therefore, the total number of carriers. To produce an electrical current, we apply an external electric field in $x$ direction, $E^x = 1.43 \times 10^9 - 10^{11}$ V/m. In our simulations, we also set the chemical potential $\mu = \hbar v_F \sqrt{\pi n} \approx 6.89 \times 10^{-20}$ kgm$^2$/s$^2 \approx 0.43$ eV, and $p = \frac{1}{3}\mu n \approx 3.12 \times 10^{-3}$ kg/s$^2$. We use the shear viscosity for doped graphene given by[9]

$$\kappa(T) = c_v n \left( \frac{\mu}{k_B T} \right)^{\frac{3}{2}}, \tag{4}$$

with $c_v \approx 1.33 \times 10^{-34}$ kgm$^2$/s $\approx \frac{5}{4}\hbar$. We couple the electronic fluid to the atomistic simulation using the same length-scale $x_0 = \Delta x_{MD} = 1$ Å and time scale $t_0 = \Delta t_{MD} = 10^{-5}$ fs. After each iteration we compute the metric tensor and the Christoffel symbols and simulate the electronic flow until we obtain the electrical current at steady state. Note that since the electronic flow is much faster than the typical speed of motion of the carbon atoms, the electrons will reach stationary solutions under adiabatic approximations. However, we still couple both time and space variations on an equal footing. The momentum change in the fluid is imposed on the atoms to ensure momentum conservation of the total system even for $\alpha \neq 1$ in Eq. (2).

## 3 Results

We perform simulations for different strains and different values of the coupling constant and measure the resistivity of the graphene sheets using Ohm's law, $\langle \rho \rangle = E^x L_y / I(t \to \infty)$, where the electrical current is given by $I(t) = \int_0^{L_y} e n(ct, x = L_x, y) U^x(ct, x = L_x, y) dy$. In Fig. 3, we observe that all our calculations of the electrical resistivity of graphene exhibit a linear dependence with temperature,

$$\rho = \gamma_s(\alpha)T + \rho_0(\alpha, L_x). \tag{5}$$

This linear dependence is in agreement with experimental measurements and theoretical predictions.[4,5] Additionally, the slope $\gamma_s(\alpha)$ only depends on the strength of the coupling constant $\alpha$ but not on the applied strain, which is also in agreement with previous works.[7] We can also observe from the inset of Fig. 3 that $\gamma_s \propto \alpha^{2.15\pm0.03}$. The factor $\gamma_s$ can be compared with the values from the Boltzmann transport theory,[5] where

$$\rho = \gamma T \equiv \frac{\pi D^2 k_B}{4e^2 \hbar \rho_m v_{ph}^2 v_F^2} T, \tag{6}$$

with $\rho_m = 7.6 \times 10^{-7}$ kg/m$^2$ being the mass density of graphene, $v_{ph}$ the phonon velocity and $D$ the deformation-potential coupling constant. Experimental and theoretical results suggest that the deformation-potential varies within the range of $10 \leq D \leq 20$ eV,[6] and phonon velocities within $2 \times 10^4 \leq v_{ph} \leq 3 \times 10^4$ m/s.[20–22] Thus, one expects $\gamma$ to be in the range $0.06 \leq \gamma \leq 0.45$ Ω/K. From our results we deduce that $0.024 \leq \alpha \leq 0.061$ to obtain results compatible with $\gamma$. The residual resistivity $\rho_0$ is $704 \pm 33$ Ω for $\alpha = 0.1$ and is a consequence of the static corrugations (ripples) present at any temperature.

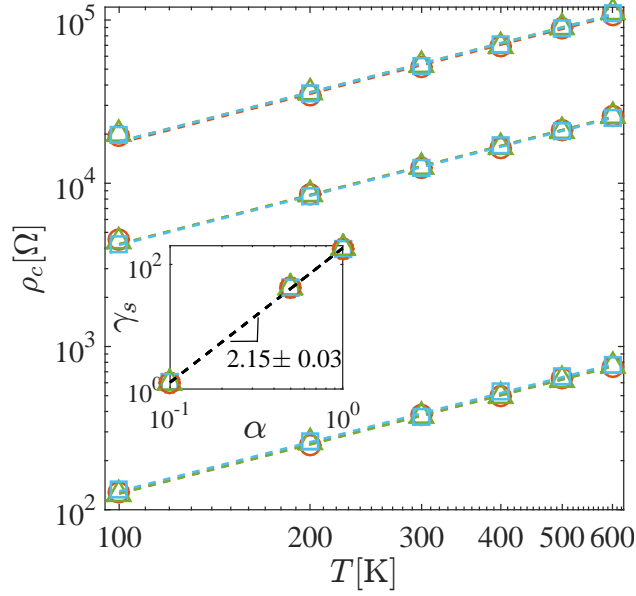**Figure 3.** Temperature dependence of the electrical resistivity of graphene due to inertial corrections for different coupling constants $\alpha$. The dashed lines correspond to the best fit for the function $\rho = \gamma_s T + \rho_0 = \rho_c + \rho_0$ for $\alpha = \{1.0, 0.5, 0.1\}$ with $\gamma_s(\alpha = 1.0) = 180 \pm 20\ \Omega/\text{K}, \gamma_s(\alpha = 0.5) = 44 \pm 7\ \Omega/\text{K}$ and $\gamma_s(\alpha = 0.1) = 1.3 \pm 0.1\ \Omega/\text{K}$. The colors represent graphene membranes with different strains where red circles stand for a graphene sheet with size $L_x = 99.2$ Å, green triangles for $L_x = 100.6$ Å and blue squares for $L_x = 102.1$ Å. Inset: Log-log plot of $\gamma_s$ dependence on $\alpha$. In both figures, the errorbars are smaller than the symbols.

These ripples stabilize the two-dimensional crystal circumventing the Mermin Wagner theorem, which states that crystalline order cannot exist in two dimensions.[23]

The linear temperature dependence observed in this set-up is related to the presence of external strain imposed by fixing the contact points at the boundary. For the study of the strain free resistivity, we have performed molecular dynamics simulations of graphene sheets without restricting the motion of the carbon atoms at the left and right boundary. We have observed that in this case, the linear behaviour of the resistivity is not recovered. Instead, in agreement with Refs.,[6,7] the data suggest a quadratic dependence of the resistivity on the temperature (see Fig. 1 of the Supplementary Information).

The existence of a resistivity points to the presence of dissipation. Recently, it has been shown that energy dissipation in flows through curved manifolds arises from the curvature.[24] The Ricci scalar (or curvature scalar) is a measure for the curvature and is given by $R^\mu_\mu = g^{\nu\sigma}(\Gamma^\mu_{\nu\sigma,\mu} - \Gamma^\mu_{\nu\mu,\sigma} + \Gamma^\delta_{\nu\sigma}\Gamma^\mu_{\mu\delta} + \Gamma^\delta_{\nu\mu}\Gamma^\mu_{\sigma\delta})$. We have analysed the Ricci scalar for different strains and temperatures and found that its maximal absolute value remains constant during time evolution and depends only on the temperature of the system (see inset of Fig. 4). As function of temperature the Ricci scalar follows a power-law with an exponent that increases with the applied strain (see main panel in Fig. 4).

We have also studied the standard deviation of the heights of our graphene sheets (which represents out-of-plane vibrations), and found that they are virtually not influenced by temperature, within the range of 100-600 K (see Fig. 2 of Supplementary Information). However, we observe that temperature does affect the bond-length distribution, as seen in Figs. 3 a-c in the Supplementary Information, meaning that it influences the in-plane vibrations of the membranes. Thus, one can conclude that the linear dependence of the resistivity with temperature is mainly due to in-plane phonons, and may be related to the lack of out-of-plane vibrations, which are suppressed when an external strain is applied (see inset of Fig. 2 in the Supplementary Information). This also explains why in the absence of strain, i.e. without the suppression of out-of-plane vibrations, the quadratic behaviour is recovered.

## 4 Conclusion

To summarise, we have shown that inertial corrections lead to a linear dependence of the electrical resistivity with temperature in suspended graphene under applied strain, which is in agreement with experimental measurements of the electrical resistivity due to electron-phonon interactions at high temperatures. To characterize the strength of the electron-phonon interaction in
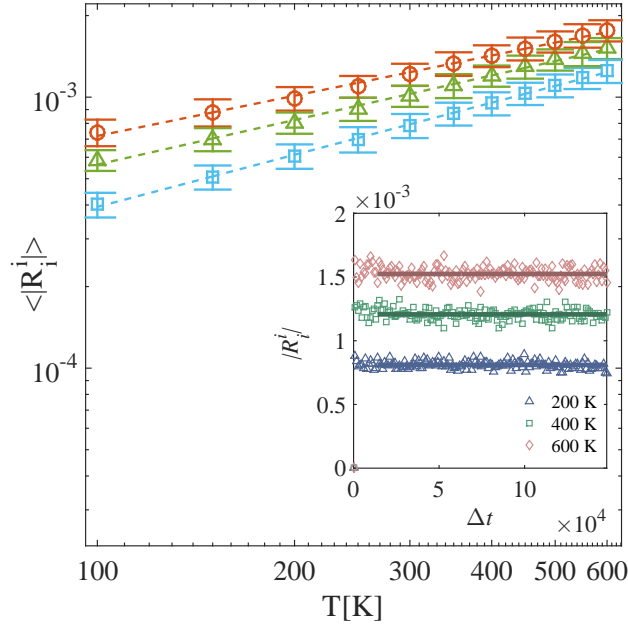
**Figure 4.** Maximal absolute value of the Ricci scalar $|R_i^i|$ for graphene membranes with distances $L_x$. Main panel: time averaged Ricci scalar $\langle |R_i^i| \rangle$ for different temperatures and distances $L_x$. Red circles correspond to $L_x = 99.2$ Å, with an exponent $0.49 \pm 0.02$. Green triangles correspond to $L_x = 100.6$ Å, with an exponent $0.55 \pm 0.03$. Blue squares correspond to $L_x = 102.1$ Å, with an exponent $0.64 \pm 0.01$. Inset panel: Time evolution of $|R_i^i|$ for graphene membranes at different temperatures for $L_x = 102.1$ Å.

our model, we have introduced a coupling constant $\alpha$, and for values of $\alpha \approx 0.05$ one expects to recover the same values of $\gamma$ known from theoretical predictions and experimental measurements. Our measured resistivity does not depend on the strength of the strain applied to the sample, however, in the complete absence of external strain it exhibits the expected quadratic temperature dependence.[6,7]

We also analysed the maximal absolute value of the curvature as function of temperature and found a power-law behaviour with an exponent that changes slightly with the applied strain. Finally, by studying the average height fluctuations of the graphene sheets under strain, we also discovered that the height fluctuations are almost temperature independent, and consequently, they seem to be uncorrelated with the changes in curvature. In contrary, the bond-length distribution (which is related to the in-plane phonons) possesses a clear temperature dependence and accounts for larger local values of curvature when increasing the temperature. In our model, larger curvature implies more energy dissipation, and consequently, larger electrical resistivity.

Our finding opens up many interesting questions, as for instance, if one can discern the influence of different types of vibrational phonons, e.g. flexural, acoustic, and optical, by studying how they introduce curvature into the hydrodynamic system. By extending our molecular dynamics simulations, one could also explore the electrical resistivity due to the electron-phonon interactions when the graphene sample is placed on a substrate.[21]

Finally, our approach can also be applied to other two- and three-dimensional crystals, where electrons are well described as Fermi liquid. In those structures, ion displacements due to phonons can induce intrinsic curvature, and consequently, energy dissipation in the electronic flow. Applying our model to other materials will be an interesting subject for future research.

## References

1. Rössler, U. *Solid state theory: an introduction* (Springer Science & Business Media, 2009).

2. Tewary, V. K. & Yang, B. Singular behavior of the debye-waller factor of graphene. *Phys. Rev. B* **79**, 125416 (2009). URL http://link.aps.org/doi/10.1103/PhysRevB.79.125416.

3. Bloch, F. Zum elektrischen widerstandsgesetz bei tiefen temperaturen. *Z. Phys.* **59**, 208–214 (1930).

4. Efetov, D. K. & Kim, P. Controlling electron-phonon interactions in graphene at ultrahigh carrier densities. *Phys. Rev. Lett.* **105**, 256805 (2010). URL http://link.aps.org/doi/10.1103/PhysRevLett.105.256805.

5. Hwang, E. H. & Das Sarma, S. Acoustic phonon scattering limited carrier mobility in two-dimensional extrinsic graphene. *Phys. Rev. B* **77**, 115449 (2008). URL http://link.aps.org/doi/10.1103/PhysRevB.77.115449.

6. Ochoa, H., Castro, E. V., Katsnelson, M. I. & Guinea, F. Temperature-dependent resistivity in bilayer graphene due to flexural phonons. *Phys. Rev. B* **83**, 235416 (2011). URL https://link.aps.org/doi/10.1103/PhysRevB.83.235416.

7. Castro, E. V. *et al.* Limits on charge carrier mobility in suspended graphene due to flexural phonons. *Phys. Rev. Lett.* **105**, 266601 (2010). URL http://link.aps.org/doi/10.1103/PhysRevLett.105.266601.

8. Müller, M., Schmalian, J. & Fritz, L. Graphene: A nearly perfect fluid. *Phys. Rev. Lett.* **103**, 025301 (2009).

9. Principi, A., Vignale, G., Carrega, M. & Polini, M. Bulk and shear viscosities of the two-dimensional electron liquid in a doped graphene sheet. *Phys. Rev. B* **93**, 125410 (2016). URL http://link.aps.org/doi/10.1103/PhysRevB.93.125410.

10. Levitov, L. & Falkovich, G. Electron viscosity, current vortices and negative nonlocal resistance in graphene. *Nature Phys.* (2016).

11. Mendoza, M., Herrmann, H. & Succi, S. Hydrodynamic model for conductivity in graphene. *Sci. Rep.* **3** (2013).

12. Mendoza, M., Herrmann, H. J. & Succi, S. Preturbulent regimes in graphene flow. *Phys. Rev. Lett.* **106**, 156601 (2011).

13. Furtmaier, O., Mendoza, M., Karlin, I., Succi, S. & Herrmann, H. J. Rayleigh-bénard instability in graphene. *Phys. Rev. B* **91**, 085401 (2015). URL http://link.aps.org/doi/10.1103/PhysRevB.91.085401.

14. Bistritzer, R. & MacDonald, A. H. Hydrodynamic theory of transport in doped graphene. *Phys. Rev. B* **80**, 085109 (2009). URL http://link.aps.org/doi/10.1103/PhysRevB.80.085109.

15. Svintsov, D., Vyurkov, V., Yurchenko, S., Otsuji, T. & Ryzhii, V. Hydrodynamic model for electron-hole plasma in graphene. *J. Appl. Phys.* **111** (2012).

16. Stuart, S. J., Tutein, A. B. & Harrison, J. A. A reactive potential for hydrocarbons with intermolecular interactions. *J. Chem. Phys* **112**, 6472–6486 (2000).

17. Koukaras, E. N., Kalosakas, G., Galiotis, C. & Papagelis, K. Phonon properties of graphene derived from molecular dynamics simulations. *Sci. Rep.* **5** (2015).

18. Cercignani, C. & Kremer, G. M. *The Relativistic Boltzmann Equation: Theory and Applications* (Boston; Basel; Berlin: Birkhauser, 2002).

19. Oettinger, D., Mendoza, M. & Herrmann, H. J. Gaussian quadrature and lattice discretization of the fermi-dirac distribution for graphene. *Phys. Rev. E* **88**, 013302 (2013). URL http://link.aps.org/doi/10.1103/PhysRevE.88.013302.

20. Borysenko, K. M. *et al.* First-principles analysis of electron-phonon interactions in graphene. *Phys. Rev. B* **81**, 121412 (2010).

21. Chen, J.-H., Jang, C., Xiao, S., Ishigami, M. & Fuhrer, M. S. Intrinsic and extrinsic performance limits of graphene devices on sio2. *Nat. Nanotechnol.* **3**, 206–209 (2008).

22. Bolotin, K., Sikes, K., Hone, J., Stormer, H. & Kim, P. Temperature-dependent transport in suspended graphene. *Phys. Rev. Lett.* **101**, 096802 (2008).

23. Mermin, N. D. Crystalline order in two dimensions. *Phys. Rev.* **176**, 250–254 (1968).

24. Debus, J.-D., Mendoza, M., Succi, S. & Herrmann, H. Curvature-induced dissipation. *arXiv preprint arXiv:1511.08031* (2015).

25. Pozrikidis, C. *Fluid dynamics: theory, computation, and numerical simulation* (Springer Science & Business Media, 2009).

## Acknowledgements

## Author Contributions

I.G., M.M. and H.H. contributed equally to the work.

## Additional Information

### Conservation equations for curved spaces

The lattice Boltzmann model for flat space reported in Ref.[19] needs to be extended in order to simulate relativistic hydrodynamics in curved spaces. This numerical model solves the following conservation equations:

$$\partial_\mu N^\mu = 0, \tag{7a}$$

$$\partial_\mu T_0^{\mu\nu} = 0, \tag{7b}$$

where $T_0^{\mu\nu}$ is the energy momentum tensor for flat space,

$$T_0^{\mu\nu} = (\varepsilon + p)\frac{U^\mu U^\nu}{v_F^2} - p\eta^{\mu\nu} + \pi^{\mu\nu}. \tag{8}$$

In curved spaces, the energy momentum tensor has to be conserved as well. However, conservation of quantities in a curved manifold needs to be expressed through covariant derivatives, instead of partial derivatives. The conservation equations for the number of particles and energy momentum tensor are given by

$$\nabla_\mu N^\mu = 0, \tag{9a}$$

$$\nabla_\mu T^{\mu\nu} = 0, \tag{9b}$$

where the covariant derivatives $\nabla_\mu$ of the 3-particle flow and energy-momentum tensor relate to the partial derivatives $\partial_\mu$ as follows:

$$\nabla_\mu N^\mu = \partial_\mu N^\mu + \Gamma^\mu_{\mu\lambda} N^\lambda, \tag{10a}$$

$$\nabla_\mu T^{\mu\nu} = \partial_\mu T^{\mu\nu} + \Gamma^\mu_{\mu\lambda} T^{\lambda\nu} + \Gamma^\nu_{\mu\lambda} T^{\mu\lambda}, \tag{10b}$$

where $\Gamma^\mu_{\mu\lambda}$ denote the Christoffel symbols which are computed with the metric tensor using

$$\Gamma^\sigma_{\mu\nu} = \frac{1}{2}g^{\sigma\rho}\left(\frac{\partial g_{\rho\mu}}{\partial x^\nu} + \frac{\partial g_{\rho\nu}}{\partial x^\mu} - \frac{\partial g_{\mu\nu}}{\partial x^\rho}\right) \quad . \tag{11}$$

Additionally, the energy momentum tensor in curved manifolds reads

$$T^{\mu\nu} = (\varepsilon + p)\frac{U^\mu U^\nu}{v_F^2} - pg^{\mu\nu} + \pi^{\mu\nu}, \tag{12}$$

where $g^{\mu\nu}$ is the metric tensor and $\pi^{\mu\nu}$ the shear-stress tensor, which can be approximated by the equation $\pi^{\mu\nu} \approx \kappa(g^{\mu\lambda}\nabla_\lambda U^\nu + g^{\nu\lambda}\nabla_\lambda U^\mu)$. Using the property that $\nabla_\mu g^{\mu\nu} = 0$, we can rewrite the covariant derivative of the energy-momentum tensor as

$$\nabla_\mu T^{\mu\nu} = \nabla_\mu T_0^{\mu\nu} + (\eta^{\mu\nu} - g^{\mu\nu})\nabla_\mu p. \tag{13}$$

Thus the conservation equations (9) expressed with the energy-momentum tensor for the flat space $T_0^{\mu\nu}$ read

$$\begin{aligned}
0 &= \nabla_\mu T^{\mu\nu} = \nabla_\mu T_0^{\mu\nu} + (\eta^{\mu\nu} - g^{\mu\nu})\nabla_\mu p \\
&= \partial_\mu T_0^{\mu\nu} + \Gamma^\mu_{\mu\lambda} T_0^{\lambda\nu} + \Gamma^\nu_{\mu\lambda} T_0^{\mu\lambda} + (\eta^{\mu\nu} - g^{\mu\nu})\partial_\mu p,
\end{aligned} \tag{14}$$

where we have used the fact that partial derivatives equal covariant derivatives when acting on scalars. At this stage we also include a temperature independent coupling constant $\alpha$ which accounts for the strength of the inertial corrections. Thus, this set of equations can be written as

$$\partial_\mu N^\mu = \alpha F_N, \tag{15a}$$

$$\partial_\mu T_0^{\mu\nu} = \alpha F_T^\nu, \tag{15b}$$

with

$$F_N = -\Gamma^\mu_{\mu\lambda} N^\lambda \tag{16a}$$

$$F_T^\nu = -\Gamma^\mu_{\mu\lambda} T_0^{\lambda\nu} - \Gamma^\nu_{\mu\lambda} T_0^{\mu\lambda} - (\eta^{\mu\nu} - g^{\mu\nu})\partial_\mu p. \tag{16b}$$

Here $F_T^\nu$ and $F_N$ can be introduced in the numerical model as external forces using the technique described in Ref.[13]

## Dimensionless quantities

In order to obtain general results we transform the hydrodynamic equations to dimensionless form and determine the dimensionless quantities that characterise our systems. We also include a force density $\vec{F}^{ext} = ne\vec{E}$ describing an external electric field $\vec{E}$ to the energy-momentum conservation equation (2).

To write the equations in a dimensionless form, we first express all relevant quantities in dimensionless form: $x = x_0 x'$, $u = u_0 u'$, $t = t_0 t'$, $\varepsilon = \varepsilon_0 \varepsilon'$, $E = E_0 E'$, $\kappa = \kappa_0 \kappa'$ $e = e' e_0$, $n = n'/x_0^2$ and $v_F = u_0 v'_F$ where all primed variables are dimensionless. Furthermore, the relation $u_0 t_0 = x_0$ holds, which allows us to write the temporal derivative $\partial_0 = (1/v_F)\partial_t = (1/v'_F u_0 t_0)\partial_{t'} = (1/v'_F x_0)\partial'_0$, and thus for $v'_F = 1$, the relation $\partial_\mu = (1/x_0)\partial'_\mu$ is also satisfied.

We divide the energy-momentum tensor in an equilibrium part and a dissipative part $T^{\mu\nu} = T^{\mu\nu(eq)} + \pi^{\mu\nu}$. The equilibrium part can be written in its dimensionless form $T^{\mu\nu(eq)} = \varepsilon_0 T'^{\mu\nu(eq)}$. Assuming that the shear-stress tensor is linearly dependent on the shear viscosity $\kappa$ [18, p. 109] and taking into account that the shear stress tensor has the same units as the energy-momentum tensor ($\kappa_0 = \frac{\varepsilon_0 x_0}{u_0}$), we get $\pi^{\mu\nu} = \kappa_0(\varepsilon_0/\kappa_0)\pi'^{\mu\nu} = \kappa_0(u_0/x_0)\pi'^{\mu\nu}$. The force densities (16) transform as $F_N = (\varepsilon_0/x_0)F'_N$ and $F_T^\nu = (\varepsilon_0/x_0)F_T'^\nu$, respectively. This can be derived from the fact that, in our case, the metric is dimensionless and thus the Christoffel symbols (as derivative of the metric) transform as $\Gamma_\sigma^{\mu\nu} = (1/x_0)\Gamma_\sigma'^{\mu\nu}$.

With the considerations above, equations (2) read

$$\frac{1}{x_0^3}\partial'_\mu N'^\mu = \frac{1}{x_0^3}F'_N, \tag{17a}$$

$$\frac{\varepsilon_0}{x_0}\partial'_\mu T'^{\mu\nu(eq)} + \frac{\kappa_0 u_0}{x_0^2}\partial'_\mu \pi'^{\mu\nu(eq)} = \frac{\varepsilon_0}{x_0}F_T'^\nu + \frac{e_0 E_0}{x_0^2}n'e'E'^\nu. \tag{17b}$$

While the first equation remains unchanged, we observe after multiplying by $(x_0/\varepsilon_0)$ that the second equation only depends on two dimensionless numbers

$$A_1 = \frac{\kappa_0 u_0}{x_0 \varepsilon_0} \text{ and } A_2 = \frac{e_0 E_0}{x_0 \varepsilon_0}. \tag{18}$$

Note that $1/A_1$ is related to the Reynolds number.[25] The parameter range of our simulations is $0.14 \leq A_1 \leq 2.05$ and $10^{-8} \leq A_2 \leq 10^{-6}$.

## Resistivity in the absence of external induced strain

The simulations of the suspended graphene samples have all non-zero strain due to the way we introduce the contact points at the left and right boundaries, i.e. the carbon atoms located at those positions are forced to remain immovable. In order to study the case of no strain we have performed simulations of graphene membranes without restricting the motion of the atoms at the boundaries. As shown in Fig. S1, in the absence of any external induced strain we observe that the linear temperature dependence of the resistivity is not recovered. Instead, the data suggest a quadratic dependence of the resistivity on the temperature, in agreement with Refs.[6,7]

## Strain induced by the contact points

All simulations are performed with the same number of carbon atoms ($N = 4114$). The atoms at the left and right boundary represent the contact points. We fix the atoms at the contact points for the simulations of the graphene membrane with external induced strain. The left and right contacts are separated at a distance $L_x$ from each other and are not allowed to move nor change the effective bond lengths of the underlying carbon atoms. The simulations are preformed for different $L_x = 99.2 - 104.2$ Å which correspond to initial effective bond lengths $a = 1.38 - 1.45$ Å.

The distance $L_x$ is related to the external imposed tension on the graphene membrane. One expects that increasing $L_x$ results in a more stretched membrane and the height fluctuations are reduced. Figure S2 confirms that the height fluctuations $\sqrt{\langle z^2 \rangle - \langle z \rangle^2}$ depend on $L_x$ and therefore also on the strain imposed on the graphene membrane. Interestingly, the height fluctuations are independent on the temperature. In contrast, the width of the effective bond length distribution presents a strong temperature dependence as shown in Figs. S3 a-c.

This finding is related to the Ricci scalar analysis (see Fig. 4 in the main article), where it has been shown that the absolute value of the Ricci scalar has a much stronger temperature dependence than a dependence on $L_x$. A higher temperature results in a broader width of the effective bond length distribution. This leads to a higher average Ricci scalar and consequently to more curvature in the system. The curvature introduces shear which is responsible for saturation of the current.
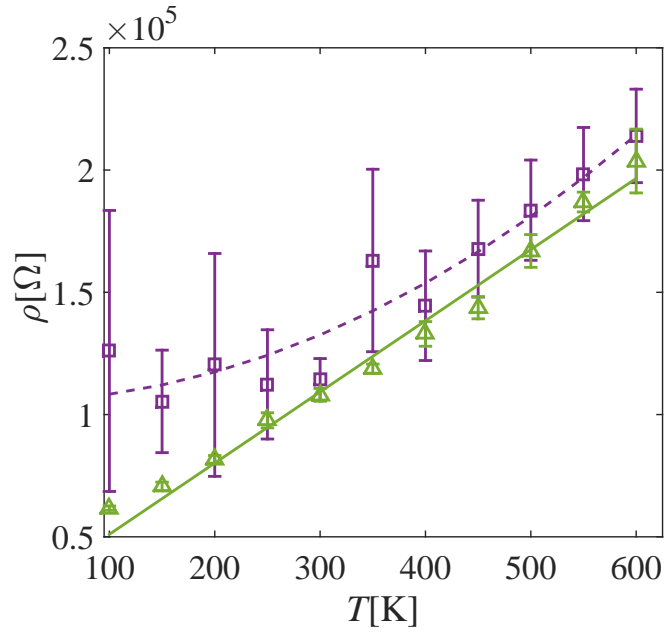
**Figure S1.** Temperature dependence of the electrical resistivity of graphene. The violet squares represents simulation results performed in complete absence of any external strain (free boundary molecular dynamics simulations, without restricting the motion of the atoms at the left and right boundary). The violet dashed line correspond to the best fit for the function $\rho = \gamma_{free}T^2 + \rho_0$. For comparison, we have also included the data of the resistivity from simulations with restriction on the left and right boundary. This data is denoted by green triangles and, in that case, the graphene has a total size $L_x = 100.6$ Å. The green line represents the best fit of this data with a linear function.



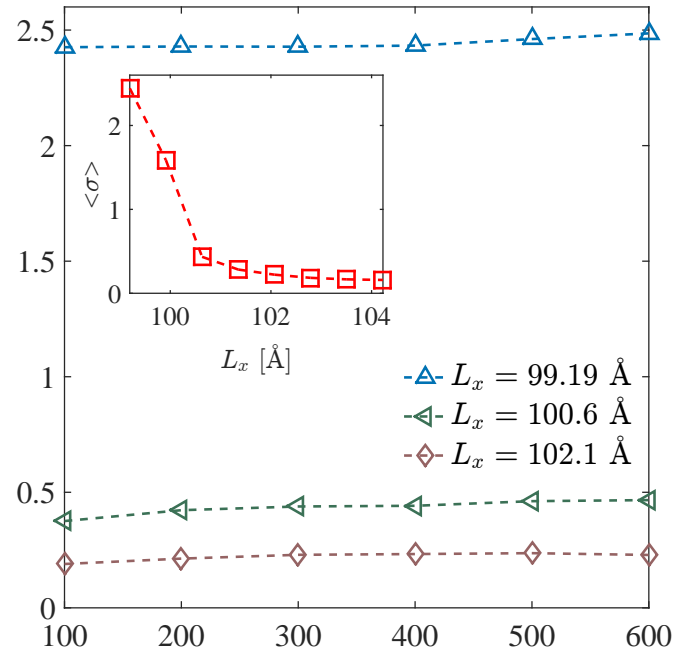**Figure S2.** Main figure: Standard deviation of the heights $\sigma$ as a function of temperature for different $L_x = \{99.2, 100.6, 102.1\}$. Inset: Temperature averaged standard deviation $\langle\sigma\rangle$ for different distances $L_x$.
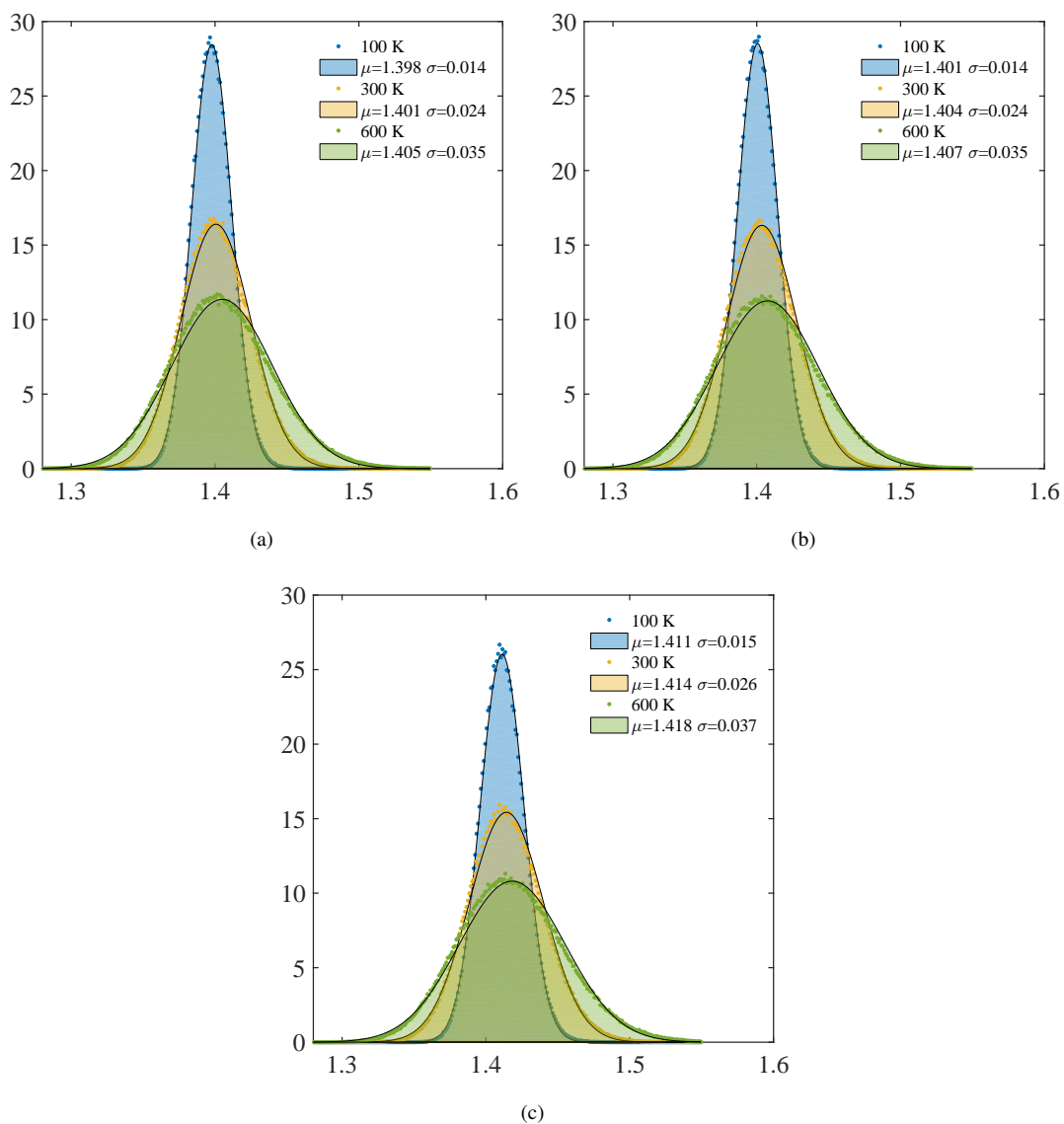
**Figure S3.** Distribution of the effective bond lengths for $L_x = 99.2$ Å (a), $L_x = 100.6$ Å (b) and $L_x = 102.1$ Å (c). The black line corresponds to a Gauss distribution with mean $\mu$ and standard deviation $\sigma$.